Fermi Gamma-Ray "Bubbles" from Stochastic Acceleration of Electrons

Philipp Mertsch and Subir Sarkar

Rudolf Peierls Centre for Theoretical Physics, University of Oxford, Oxford OX1 3NP, United Kingdom

(Received 26 April 2011; revised manuscript received 20 May 2011; published 23 August 2011)

Gamma-ray data from Fermi Large Area Telescope reveal a bilobular structure extending up to ~50° above and below the Galactic Center. It has been argued that the gamma rays arise from hadronic interactions of high-energy cosmic rays which are advected out by a strong wind, or from inverse-Compton scattering of relativistic electrons accelerated at plasma shocks present in the bubbles. We explore the alternative possibility that the relativistic electrons are undergoing stochastic 2nd-order Fermi acceleration by plasma wave turbulence through the entire volume of the bubbles. The observed gamma-ray spectral shape is then explained naturally by the resulting hard electron spectrum modulated by inverse-Compton energy losses. Rather than a constant volume emissivity as in other models, we predict a nearly constant surface brightness, and reproduce the observed sharp edges of the bubbles.

DOI: 10.1103/PhysRevLett.107.091101 PACS numbers: 98.70.Rz, 95.30.Qd, 98.35.Jk, 98.70.Sa

Recent data from the Fermi Large Area Telescope satellite have revealed [1,2] the presence of giant gamma-ray lobes ~40° wide, extending up to ~50° above and below the Galactic Center (GC). The energy spectrum of the emission from these "Fermi bubbles" is $dN/dE \sim E^{-2}$ from ~1–200 GeV, i.e., considerably harder than conventional foregrounds. Furthermore, the bubbles exhibit an almost constant surface brightness with hard edges. While the template subtraction technique used to reveal the bubbles may not be appropriate at these high energies, the resulting systematic effects are not easy to assess. However, the bubbles do correlate with features at other wavelengths; viz. data from the ROSAT x-ray satellite [3] show a limb-brightened, conical structure close to the Galactic plane which coincides with the edges of the Fermi bubbles. The bubbles also line up with a claimed excess in microwaves at lower bilobular latitudes—the so-called WMAP haze [4].

Although extended lobes have long been seen in other galaxies in radio, x rays, and gamma rays, their presence in the Milky Way is surprising. There is no radio emission from these bubbles, unlike those seen in the majority of active galaxies. Moreover their morphology (symmetry with respect to the bilobular plane and alignment with the GC) suggests that the central supermassive black hole is the energy source. However it is supposedly in a quiescent state so it is a puzzle how the bubbles have formed; understanding this would provide an excellent probe of this region which is otherwise obscured by the bilobular disk. The bubbles may play an important role in the dynamics of our Galaxy and constitute a source of cosmic rays (CRs). While they are prominent at high bilobular latitudes, the associated signal close to the plane, while uncertain, constitutes a background for indirect dark matter searches. It is therefore important to understand and model the origin of the nonthermal emission from the bubbles.

While the mechanism responsible for the formation of the bubbles is not necessarily the same as the source of the gamma-ray emission today, it is useful to recall their general properties. The limb-brightened shell in the ROSAT data implies a shock front at the bubble edges, but from the observed cavity hot low density gas is inferred to fill the bubble interiors. Assuming a low density ($n \sim 10^{-2}$ cm^{-3}) gas at $T \sim 2$ keV and shock velocities $U \lesssim 1000$ km s^{-1}, the energy is estimated to be $\sim 10^{54-55}$ erg in hot gas and the age to be $\sim 10^{7}(U/1000\ \mathrm{km\,s^{-1}})$yr [1]. Suggested mechanisms for providing such an energy on this time scale include jets emanating from the central black hole [5], star-forming regions close to the GC [6], or repeated star accretion onto the central black hole [7].

The observed gamma rays may be generated by hadronic interactions of high-energy CR protons or nuclei (i.e., π^0 decay) provided that the ambient gas density is not too low. It has been proposed [6] that protons and nuclei accelerated by supernova remnants in star-forming regions very close to the GC could be advected by a strong wind out to kiloparsec distances above the plane. If the confinement time is larger than all other time scales, the hard power-law spectrum of the gamma rays would simply reflect the source spectrum of the protons. The spectral shoulder at ~1 GeV can be explained by the pion bump.

Another possible mechanism is the inverse-Compton (IC) scattering of high-energy electrons off ambient radiation fields [CMB, far infrared (FIR), and optical/UV]. The spectral feature seen at a few hundred GeV may reflect a cutoff in the electron spectrum at a similar energy, either due to energy losses or due to the competition between an energy-dependent acceleration rate and the finite age of the bubbles. Furthermore, the WMAP haze may well arise from synchrotron radiation of these electrons in the ambient magnetic field. A crucial question then is how the electrons are accelerated.

The standard paradigm for the acceleration of Galactic CRs is diffusive shock acceleration (DSA) by the 1st-order Fermi process, which predicts power-law source spectra with index close to -2. There are at least four regions where shocks may be present: at the GC, inside a jet emanating from the GC, at its termination shock at the upper or lower edges of the bubbles, and at the shocked exterior of the bubbles. So far there is only evidence from ROSAT data for a shock at the bubble exterior. In any case, presuming diffusive-convective transport from the acceleration site through the bubble volume, it is difficult to see how the electrons can maintain their hard source spectrum. The energy loss time due to IC scattering for the $\mathcal{O}$(TeV) energy electrons present throughout the bubble is only a few times 10^5 yr; however, even with a convection velocity as high as $v \sim 1000\ \mathrm{km\,s^{-1}}$, it would take the electrons 10^7 yr to cross the required distance of $\mathcal{O}(10)$kpc. The leptonic source model [7] therefore invokes hundreds of consecutive shocks in order to fill the whole bubble with freshly accelerated electrons. This would however imply a constant volume emissivity which in projection would yield a characteristic bumplike profile with soft edges, in contrast to what is observed.

We consider instead the stochastic acceleration of high-energy electrons by isotropic, large-scale turbulence in magnetosonic waves [8]. Such 2nd-order Fermi acceleration accounts well for the radio emission from supernova remnants [9,10] and the extended lobes of radio galaxies [11], and may even be the acceleration mechanism for ultrahigh-energy cosmic rays [12]. The shock front at the bubble edges suggests that they may have been powered by a jet emanating from the massive black hole at the GC that was active a few million years ago. MHD modeling [5] of a two-component plasma explains the formation of a bubble by a light but overpressured jet with $\sim$16% of the Eddington luminosity, and also predicts a shock coincident with the ROSAT shell. Plasma instabilities, in particular, Rayleigh-Taylor and Kelvin-Helmholtz instabilities, would then generate turbulence at the outer shock that is convected into the bubble interior by the downstream plasma flow. The free energy dissipation rate $Q = C_1 \rho u^3/L$ is determined by the scale of turbulence injection, L, and the eddy velocity at the injection scale, $u = v_{\mathrm{edd}}(L)$, where $C_1 = 0.485$ is the one-dimensional Kolmogorov constant [10]. The energy density at scale k is then given by $W(k) = (u^2/4\pi) L^{-2/3} k^{-11/3}$. Applying the Rankine-Hugoniot conditions at the shock, the eddy velocity at the injection scale, u, and the magnetosonic phase velocity, v_F, vary with the distance $x = \xi L$ from the shock as [10]

$$u(\xi) = \frac{U}{4} \frac{1}{C_1 \xi/3 + a^{-1/2}}, \tag{1}$$

$$v_F(\xi) = \frac{U}{4}\left(5 - \frac{5}{3(C_1\xi/3)^2} + 4\frac{v_A^2}{U^2}\right)^{1/2}, \tag{2}$$

where U is the shock velocity, v_A the Alfvén velocity (which we assume to be constant and equal to the speed of sound $v_{s,0}$ at the shock), and $a = 3$–$16 v_{s,0}^2/U^2$.

At small enough scales $l_d = 1/k_d = L(v_A/u)^3$, the kinetic energy of the turbulence becomes comparable to the magnetic field energy, $v_{\mathrm{edd}}(l_d) \approx v_A$, resulting in transit-time damping. With parameters to be justified below, it turns out that for all energies of interest, the gyro-radius r_g of the electrons is always smaller than this dissipation scale l_d such that gyro-resonant interactions with magnetosonic turbulence are not possible. Therefore, we adopt the dissipation scale to be the mean-free path, thus rendering the spatial diffusion coefficient $D_{xx} = l_d c/3$ energy independent. If additional small-scale turbulence is present (possibly responsible for spatial diffusion [8]), then the mean-free path can be smaller.

The temporal evolution of $n(t, p)dp$, the number density of electrons with momentum between p and $(p + dp)$, is dictated by the Fokker-Planck equation [13],

$$\frac{\partial n}{\partial t} - \frac{\partial}{\partial p}\left(p^2 D_{pp} \frac{\partial}{\partial p}\frac{n}{p^2}\right) - \frac{n}{t_{\mathrm{esc}}} + \frac{\partial}{\partial p}\left(\frac{dp}{dt} n\right) = 0, \tag{3}$$

where the diffusion coefficient in momentum for scattering by fast magnetosonic waves is [8]

$$D_{pp} = p^2 \frac{8\pi D_{xx}}{9} \int_{1/L}^{k_d} dk \frac{W(k) k^4}{v_F^2 + D_{xx}^2 k^2}. \tag{4}$$

The second term in Eq. (3) describes diffusion in momentum as well as systematic energy gains on the characteristic time scale $t_{\mathrm{acc}} \sim p^2/D_{pp}$, which is also energy independent. Diffusive losses from the acceleration region can be accounted for by escape on the time scale $t_{\mathrm{esc}} = L^2/D_{xx}$. Finally, the electrons lose energy through IC scattering and synchrotron radiation which are both accounted for by the energy-dependent cooling time $t_{\mathrm{cool}} = -p/(dp/dt)$.

Because of the energy-independent spatial diffusion coefficient, the so-called hard-sphere approximation [14] is exact which makes the problem amenable to analytical solution. If the escape rate is not much bigger than the acceleration rate, i.e., $t_{\mathrm{acc}} \lesssim t_{\mathrm{esc}}$, the steady-state spectrum $n(p)$ at a fixed position can be described as a power law with a spectral cutoff above (and pileup around) a characteristic momentum p_{eq}, defined by $t_{\mathrm{acc}}(p_{\mathrm{eq}}) \equiv t_{\mathrm{cool}}(p_{\mathrm{eq}})$ [15]:

$$n(p) \propto \begin{cases} p^{-\sigma} & \text{for } p \ll p_{\mathrm{eq}}, \\ p^2 e^{-p/p_{\mathrm{eq}}} & \text{for } p \sim p_{\mathrm{eq}}. \end{cases} \tag{5}$$

The spectral index, $-\sigma = 1/2 - \sqrt{9/4 + t_{\mathrm{acc}}/t_{\mathrm{esc}}}$, is determined by the ratio of acceleration and escape times, and asymptotically approaches -1 as $t_{\mathrm{acc}}/t_{\mathrm{esc}} \to 0$.

Anticipating that the acceleration time is smaller than the lifetime $t_{\rm life}$ of the bubbles, we justify the use of the steady-state solution for acceleration volumes that are being advected with the downstream plasma. It is sufficient to consider the variation of the acceleration and escape times with the distance from the shock, which determines the spatial dependence of the electron spectrum. This hierarchy of time scales ensures that the variation with position happens adiabatically, such that the electrons can always relax to their steady-state spectrum. In the upper panel of Fig. 1 we show the different time scales in the problem as a function of energy for the parameters discussed below. Although $t_{\rm cool}$ is of the same order as the dynamical time $t_{\rm conv}$ around 10 GeV, we expect that the steady-state spectrum is reached in a time $t \sim t_{\rm acc}$, as has been shown explicitly [16] for ionization losses.

The relative normalization of the electron spectrum is fixed by noting that the total energy in relativistic electrons at any position is a constant fraction of the free energy dissipated along with the downstream plasma up until this position. This does not however fix the absolute normalization which depends on the microphysics of the acceleration process, in particular, the injection mechanism. We determine the gamma-ray volume emissivity due to IC scattering off the CMB, FIR, and optical/UV backgrounds adopting the interstellar radiation fields from GALPROP [17] at a reference height of 4 kpc above the GC. For the parameters discussed below we show the electron spectrum $E^2 n_{e^-}$ for different distances from the shock in the lower panel of Fig. 1.

We now discuss the parameters that can reproduce the observed gamma-ray flux—both its spectrum and morphology. Kelvin-Helmholtz instabilities have been observed to be generated on kpc scales in MHD simulations of the Fermi bubble gas [5], so we choose the scale of turbulence generation to be $L = 2$ kpc. The shock velocity can in principle be determined kinematically from the variation of its position with time [the shock needs $\sim 50(U/10^8\ {\rm cm\,s^{-1}})$yr to move a distance corresponding to the $1''$ resolution of the Chandra x-ray observatory] or possibly inferred from the observed shock heating. We fix $U = 2.6 \times 10^8\ {\rm cm\,s^{-1}}$, a value consistent with MHD simulations [5]. Finally the Alfvén velocity is given by the square root of the ratio of magnetic field energy density to thermal plasma energy density: $\beta_A = v_A/c = \sqrt{U_B/U_\rho}$. Hence $\beta_A > 2.8 \times 10^{-4}$ for an estimated upper limit on the thermal gas density $n \lesssim 10^{-2}\ {\rm cm^{-3}}$ [1] and a magnetic field $B = 4\ \mu$G (suggested by radio observations of the edge-on spiral galaxy NGC 891 [18]). We adopt $\beta_A = 5 \times 10^{-4}$. The gyro radius of relativistic electrons is then $\sim 7.5 \times 10^{11}(B/4\ \mu{\rm G})^{-1}(E/{\rm GeV})$ cm, which is much smaller than the dissipation length $l_d > 8 \times 10^{19}(L/{\rm kpc})(U/10^8\ {\rm cm\,s^{-1}})^{-3}(\beta_A/10^{-3})^3$ cm even for $\mathcal{O}(10)$TeV electrons, thus confirming the energy independence of the acceleration and escape time. With these parameters we find a total energy in electrons above 100 MeV of $\sim 10^{51}$ erg which is over 5 orders of magnitude smaller than the required energy in protons in the hadronic emission model [6].

In Fig. 2 we show our predicted flux $E^2 J_\gamma$ of high-energy gamma rays (averaged over the surface of the Fermi bubbles) as a function of energy, and compare it to the data [1] as well as to the hadronic [6] and leptonic DSA [7] models. Note that our hard electron spectrum nicely reproduces the spectral shoulder around a GeV and the cutoff at a few hundred GeV. We show how the total gamma-ray flux is made up of contributions from IC scattering on the CMB, FIR, and optical/UV backgrounds (dash-dotted line, from

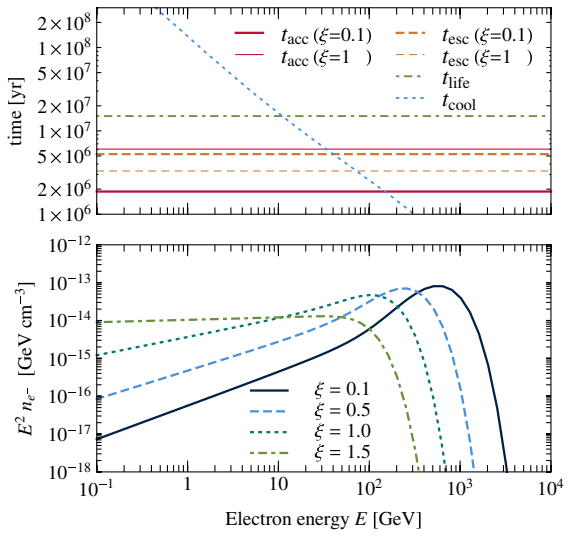

FIG. 1 (color online). Relevant time scales (top) and the electron spectrum (bottom), at various distances $x = \xi L$ from the shock.

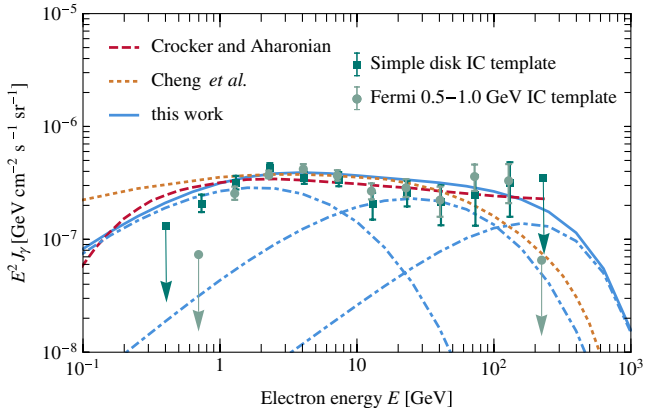

FIG. 2 (color online). The average gamma-ray flux J_γ from the Fermi bubbles [1] compared to the spectrum from our model (the contributions from inverse-Compton scattering on the CMB, FIR, and optical/UV backgrounds are shown from left to right as dash-dotted lines). The spectra from a hadronic [6] (dashed line) and a leptonic DSA model [7] (dotted line) are also shown.

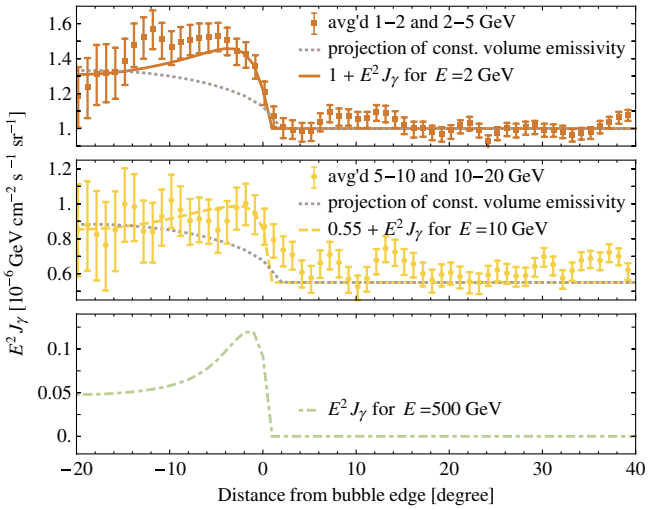

FIG. 3 (color online). The gamma-ray intensity as a function of distance from the bubble edge [1] is compared with our model predictions at 2 GeV (solid line), 10 GeV (long dashed line), and 500 GeV (dash-dotted line). The dotted line indicates the expected profile for both the hadronic model [6] and the leptonic DSA model [7].

left to right). Since we expect the FIR and optical/UV contributions to decrease rapidly with distance from the disk, the emission from high latitudes should cut off above tens of GeV—a potential test of the model. In Fig. 3 we compare the data with the predicted gamma-ray intensity at 2 and 10 GeV as a function of distance from the bubble edge (calculated as in Ref. [1], i.e., averaging over arcs of great circles converging at the bubble center). This test has not been done before; it is seen that our model matches the almost constant intensity in the interior with hard edges, in contrast to the hadronic [6] and leptonic DSA [7] models. We also show our model prediction for higher (500 GeV) gamma-ray energies; the presence of sharp edges in gamma rays can be tested by the forthcoming Cherenkov Telescope Array.

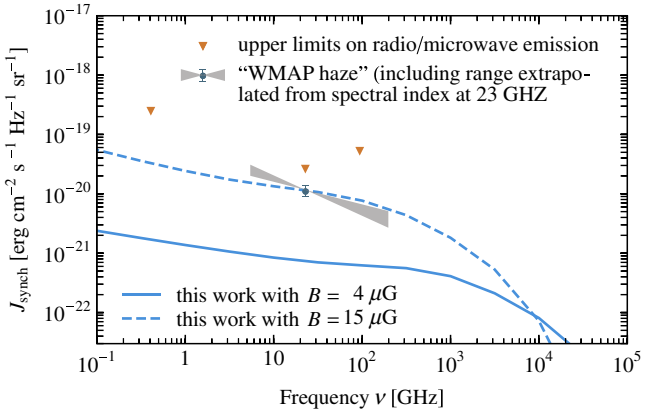

FIG. 4 (color online). Our model prediction for the synchrotron flux at $(\ell, b) = (0°, 25°)$, for two assumed magnetic field values, compared to the inferred spectrum of the WMAP haze [4].

The energy dependence of the profiles reflects the spatial variation of the electron spectrum with distance from the shock (see also Fig. 1). Close to the shock, the acceleration time is relatively small such that the spectrum is very hard, $p_{\rm eq}$ is large, and the spectral bump and cutoff appear at high energies. Further away from the shock, $t_{\rm acc}$ becomes larger and the spectrum softer, while the bump and cutoff move to lower energies. The emission of the highest energy gamma rays (due to the highest energy electrons) is thus localized close to the shock and results in the limb-brightening above a few hundred GeV. Intermediate energy gamma rays can be produced from both high and intermediate energy electrons which have a more extended distribution, leading to a flatter intensity profile.

While the WMAP haze [4] has not been observed in polarized emission [19] and may just be an artifact of the template subtraction [20], it has been proposed as a physical counterpart of the Fermi bubbles [1]. However, as seen in Fig. 4, the expected synchrotron flux in our model is of the required amplitude only if the magnetic field is as strong as 15 μG, several kpc from the plane.

The hadronic model predicts a detectable flux of neutrinos for the proposed Mediterranean km^3 neutrino telescope [6]. However, the observed bubble profile disfavors this model (as well as the leptonic DSA model) and instead favors 2nd-order Fermi acceleration of electrons, which would not generate any neutrinos.

[1] M. Su, T. R. Slatyer, and D. P. Finkbeiner, Astrophys. J. **724**, 1044 (2010).
[2] Fermi, http://www.nasa.gov/fermi; see also G. Dobler *et al.*, Astrophys. J. **717**, 825 (2010).
[3] S. L. Snowden *et al.*, Astrophys. J. **485**, 125 (1997).
[4] D. P. Finkbeiner, arXiv:astro-ph/0409027; G. Dobler and D. P. Finkbeiner, Astrophys. J. **680**, 1222 (2008).
[5] F. Guo and W. G. Mathews, arXiv:1103.0055.
[6] R. M. Crocker and F. Aharonian, Phys. Rev. Lett. **106**, 101102 (2011).
[7] K. S. Cheng *et al.*, arXiv:1103.1002 [Astrophys. J. Lett. (to be published)].
[8] V. S. Ptuskin, Sov. Astron Lett. **14**, 255 (1988).
[9] J. S. Scott and R. A. Chevalier, Astrophys. J. Lett. **197**, L5 (1975); R. Cowsik and S. Sarkar, Mon. Not. R. Astron. Soc. **207**, 745 (1984).
[10] Z. Fan, S. Liu, and C. L. Fryer, Mon. Not. R. Astron. Soc. **406**, 1337 (2010).
[11] C. Lacombe, Astron. Astrophys. **54**, 1 (1977); A. Achterberg, *ibid.* **76**, 276 (1979); J. A. Eilek, Astrophys. J. **230**, 373 (1979).
[12] M. J. Hardcastle *et al.*, Mon. Not. R. Astron. Soc. **393**, 1041 (2009); F. Fraschetti and F. Melia, *ibid.* **391**, 1100 (2008); S. O'Sullivan, B. Reville, and A. M. Taylor, *ibid.* **400**, 248 (2009).
[13] V. L. Ginzburg, Uspekhi z. nauk. **62**, 34 (1957).
[14] N. S. Kardashev, Sov. Astron. **6**, 317 (1962).
[15] L. Stawarz and V. Petrosian, Astrophys. J. **681**, 1725 (2008).

[16] P. A. Becker, T. Le, and C. D. Dermer, Astrophys. J. **647**, 539 (2006).
[17] T. A. Porter and A. W. Strong, *Proc. 29th Int. Cosmic Ray Conf., Pune* (2005), Vol. 4, p. 77, http://icrc2005.tifr.res.in/; See http://galprop.stanford.edu/resources.php?option=data.
[18] R. Beck *et al.*, Astron. Astrophys. **77**, 25 (1979).
[19] B. Gold *et al.*, Astrophys. J. Suppl. Ser. **192**, 15 (2011).
[20] P. Mertsch and S. Sarkar, J. Cosmol. Astropart. Phys. 10 (2010) 019.